Provided for non-commercial research and education use.
Not for reproduction, distribution or commercial use.

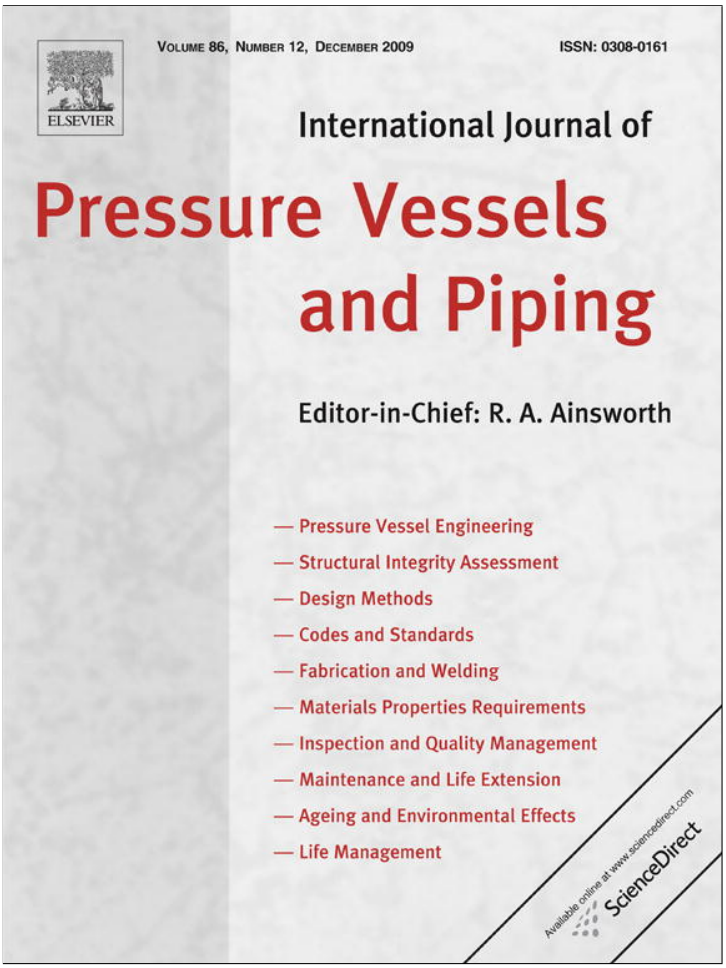

This article appeared in a journal published by Elsevier. The attached copy is furnished to the author for internal non-commercial research and education use, including for instruction at the authors institution and sharing with colleagues.

Other uses, including reproduction and distribution, or selling or licensing copies, or posting to personal, institutional or third party websites are prohibited.

In most cases authors are permitted to post their version of the article (e.g. in Word or Tex form) to their personal website or institutional repository. Authors requiring further information regarding Elsevier's archiving and manuscript policies are encouraged to visit:

http://www.elsevier.com/copyright

Author's personal copy

International Journal of Pressure Vessels and Piping 86 (2009) 787–797

Contents lists available at ScienceDirect

International Journal of Pressure Vessels and Piping

journal homepage: www.elsevier.com/locate/ijpvp

Effects of crack depth and specimen size on ductile crack growth of SENT and SENB specimens for fracture mechanics evaluation of pipeline steels

J. Xu [a,c], Z.L. Zhang [a,*], E. Østby [b], B. Nyhus [b], D.B. Sun [c]

[a] Department of Structural Engineering, Norwegian University of Science and Technology (NTNU), Richard Birkelands vei 1a, N-7491 Trondheim, Norway
[b] SINTEF, Materials and Chemistry, N-7465 Trondheim, Norway
[c] School of Materials Science and Engineering, University of Science and Technology Beijing (USTB), 100083 Beijing, China

ARTICLE INFO

Article history:
Received 5 January 2009
Received in revised form
23 November 2009
Accepted 3 December 2009

Keywords:
Crack tip constraint
Ductile fracture
Crack growth resistance
The complete Gurson model
Size effect

ABSTRACT

A strong geometry dependence of ductile crack growth resistance emerges under large scale yielding. The geometry dependence is associated with different levels of crack tip constraint conditions. However, in a recent attempt to identify appropriate fracture mechanics specimens for pipeline steels, an "independent" relationship between the crack growth resistance curves and crack depths for SENT specimens has been observed experimentally. In this paper, we use the complete Gurson model to study the effects of crack depth and specimen size on ductile crack growth behavior. Crack growth resistance curves for plane strain, mode I crack growth under large scale yielding conditions have been computed. SENB and SENT specimens with three different specimen sizes, each specimen size with three different crack depths, have been selected. It has been found that crack tip constraint (Q-parameter) has a weak dependence on the crack depth for specimens in the low constraint regime.

© 2009 Elsevier Ltd. All rights reserved.

1. Introduction

It is now well understood that crack tip constraints due to specimen geometries, loading modes and yield strength mismatches as well as residual stresses [1–10] affect the stress distribution around a crack and consequently preclude the use of a single parameter characterization of the crack tip stress field. A second parameter based on the elastic T-stress has been proposed by Betegon and Hancock [11] to describe the crack tip stress field. For elastic–plastic problems, O'Dowd and Shih [12,13] proposed a J–Q formulation to characterize the crack tip stress field and quantify constraint levels for various geometries and loading configurations in elastic–plastic materials, where J sets the deformation level and Q is a stress triaxiality parameter.

The purpose of studying constraint is to find an appropriate parameter(s) to characterize the crack tip stress–strain fields, so that fracture toughness results can be transferred from one test geometry to another. This transferability of material toughness remains a key issue in applications of fracture mechanics to assess the integrity of structural components, in particular pipelines.

From fracture mechanics theory, it has been known that fracture toughness will saturate when the crack tip constraint (characterized by Q-parameter) is high. It will increase with the decrease of crack tip constraint (see Ref. [14]). Furthermore, fracture mechanics testing consistently reveals the significant effects of specimen geometry and loading mode (tension vs. bending), associated with different levels of crack tip constraint, on measured resistance curves (for typical examples, see Refs. [15–18]).

Crack-like defects in pipe systems often develop during fabrication or in-service operation. The standard single edge notched bending (SENB) specimen with crack depth of $a/W = 0.5$ has a significantly higher geometry constraint than actual pipes with circumferential surface cracks, which therefore introduces a high degree of conservatism in engineering critical assessment (ECA) of pipes [19]. Recently, a so-called single edge notched tension (SENT) methodology [20–23] by identifying a SENT specimen(s) to match the crack tip constraint of cracked pipe sections have been developed. Most of the fracture toughness data generated from SENT specimens are performed in accordance with the "Recommended practice DNV-RP-F108" [23]. This guideline specifies that it is safe to use SENT specimens as long as the crack depth in the SENT specimen is deeper than the cracks in the pipe.

However, in a recent attempt to identify appropriate fracture mechanics specimens for pipeline steels, an "independent" relationship between the crack growth resistance curves and crack depths for the SENT specimens has been observed from experimental study (see Fig. 1 [22]).

* Corresponding author. Tel.: +47 73592530.
E-mail address: zhiliang.zhang@ntnu.no (Z.L. Zhang).

0308-0161/$ – see front matter © 2009 Elsevier Ltd. All rights reserved.
doi:10.1016/j.ijpvp.2009.12.004

Author's personal copy

Nomenclature

a	crack depth
Δa	amount of crack growth
W	specimen width
$2L$	specimen length
E	Young's modulus
ν	Poisson's ratio
n	strain hardening exponent
σ_0	yield stress
σ_f	flow stress
σ_m	mean normal stress component
ε_0	yield strain
ε_p	equivalent plastic strain
$\boldsymbol{\varepsilon}^{\mathbf{p}}$	plastic strain tensor
$\mathbf{I}$	second-order unit tensor
q	von Mises stress
q_1, q_2	constants introduced to modify the Gurson model
f	void volume fraction
f_0	initial void volume fraction
f_c	critical void volume fraction
f_F	void volume fraction at final failure
SENB	single edge notched bending
SENT	single edge notched tension
CTOD	crack tip opening displacement
CGM	complete Gurson model
ECA	engineering critical assessment

To obtain a deep understanding of the relationship between the geometry constraint and ductile fracture resistance of pipeline steels, a numerical study has been carried out to investigate the effects of crack depth and specimen size for SENT and SENB specimens on ductile crack growth behavior. The complete Gurson model (CGM) developed and implemented by Zhang [24] has been utilized to predict the crack growth resistance curves in this study.

The paper is organized as follows. In Section 2, the complete Gurson model used for studying ductile crack growth behavior is briefly described. Numerical procedure, including the material properties, specimen geometries and finite element models are presented in Section 3. Details of the numerical analyses, results and discussion are included in Section 4. The paper is closed with concluding remarks.

2. The complete Gurson model (CGM)

Ductile crack growth in metals is a result of nucleation, growth and coalescence of microvoids. A large number of investigations have been made in developing the constitutive models for elastic–plastic materials incorporating void mechanisms and the best model appears to be the one originally introduced by Gurson [25] and later modified by Tvergaard and Needleman [26–28], which thus is mostly often referred as Gurson–Tvergaard–Needleman (GTN) model.

The yield function of the Gurson–Tvergaard–Needleman model has the following form:

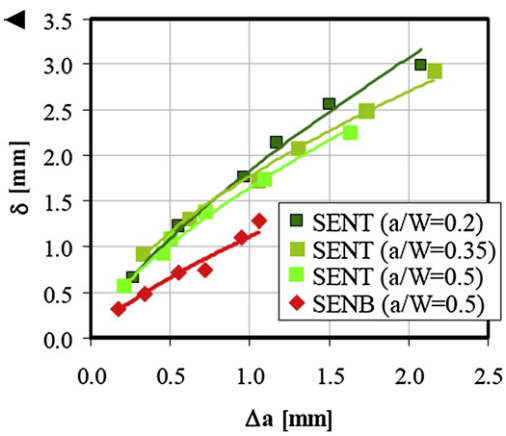

Fig. 1. CTOD-R curves for SENT specimens with different crack depths compared with the standardized SENB specimen [22].

$$\phi\left(q,\sigma_f,f,\sigma_m\right)=\frac{q^2}{\sigma_f^2}+2q_1 f\cosh\left(\frac{3q_2\sigma_m}{2\sigma_f}\right)-1-(q_1 f)^2=0 \quad (1)$$

where q is the von Mises stress, σ_f is the flow stress which is a function of plastic strain, f is the void volume fraction and σ_m is the mean normal stress component. q_1 and q_2 are constants introduced by Tvergaard [26,27] to modify the original Gurson model. In this study, fixed values of $q_1=1.5$ and $q_2=1.0$ are applied as usually been taken in the GTN model in this work.

Due to the incompressible nature of the matrix material, the growth of existing voids can be expressed as:

$$df_{\text{growth}} = (1-f)d\boldsymbol{\varepsilon}^{\boldsymbol{p}} : \mathbf{I} \quad (2)$$

where $\boldsymbol{\varepsilon}^{\boldsymbol{p}}$is the plastic strain tensor and $\mathbf{I}$ is the second-order unit tensor. In this work, the increase in void volume fraction is assumed to be due solely to the growth of existing voids (as assumed by introducing initial void volume fraction,f_0), and no void nucleation is introduced in the analyses.

There are two different coalescence criteria used in the literature, the so-called critical void volume fraction criterion and Thomason's plastic limit load model [29]. The so-called critical void volume fraction criterion empirically used in the Gurson model assumes that the void coalescence occurs when a critical void volume fraction, f_c, has been reached. The void coalescence ends when the void volume fraction reaches another value – the void volume fraction at final failure, f_F. Tvergaard and Needleman [28] introduced a function that artificially amplifies void growth to simulate the void coalescence process:

$$f^* = \begin{cases} f & \text{for } f \le f_c \\ f_c + \frac{f_u^* - f_c}{f_F - f_c}(f - f_c) & \text{for } f > f_c \end{cases} \quad (3)$$

where $f_u^* = 1/q_1$. When $f > f_c$, f^* replaces f in Eq. (1).

In deriving the Gurson model, only homogeneous deformation has been considered. Later Thomason [29] suggested that the localized deformation mode of void coalescence should be treated differently. There is a "competition" between these two deformation modes in Thomason's plastic limit load model. At the beginning, small voids could deform independently with each other. With further development of plastic deformation, the stress for localized deformation decreases and therefore the localized deformation mode will eventually become dominant.

By combining the Gurson model and Thomason's plastic limit load model, a complete Gurson model (CGM) was obtained by Zhang [24], which can simulate the whole ductile fracture process, including void nucleation, growth and coalescence. It should be

Author's personal copy

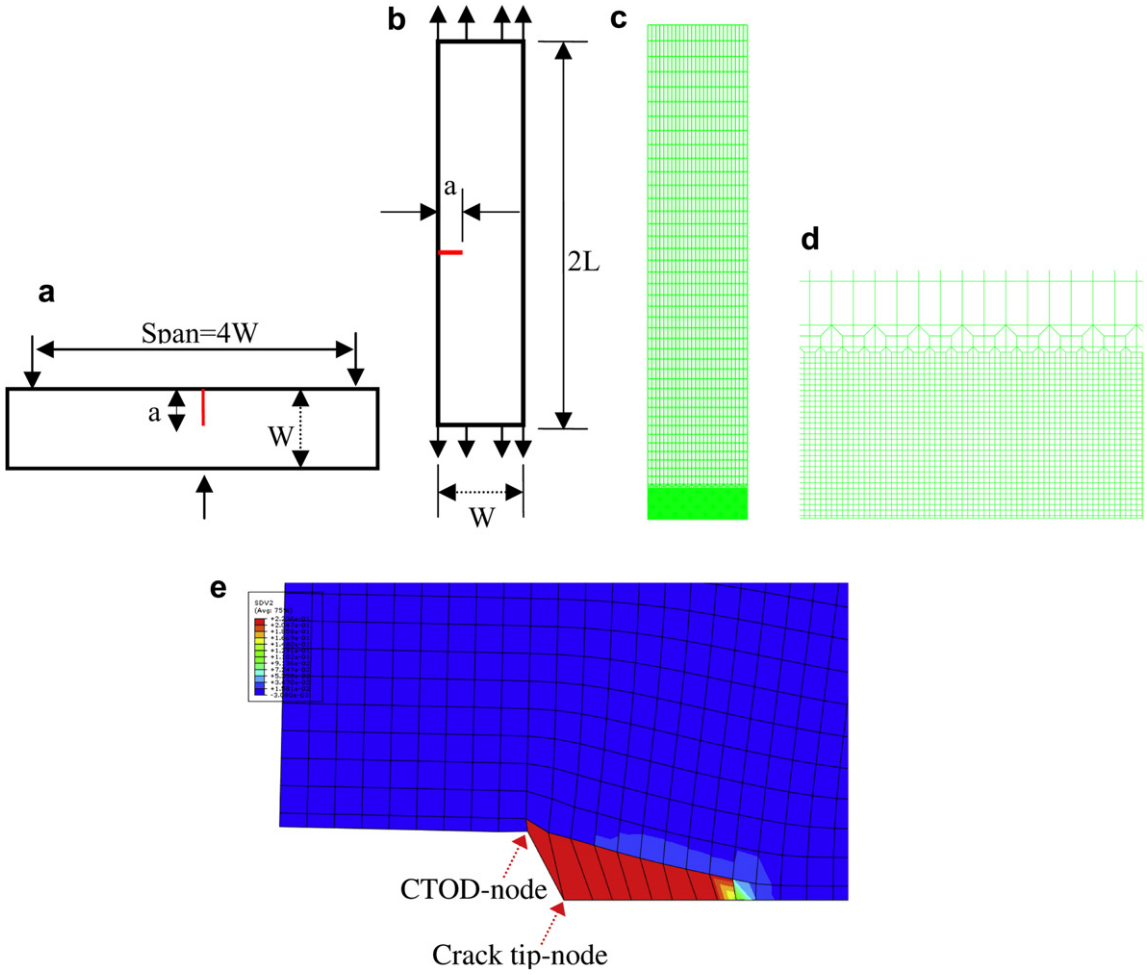

Fig. 2. Schematic plot of the specimens. (a) SENB; (b) SENT; (c) finite element mesh; (d) crack tip mesh arrangement; (e) CTOD-node.

noted that the critical void volume fraction f_c was automatically determined by the CGM, and the void volume fraction at final failure, $f_F = 0.20 + 2f_0$, has been used in the present study. The complete Gurson model was implemented into ABAQUS [30] using a user material subroutine UMAT developed by Zhang [31–33]. A free copy of the ABAQUS UMAT code can be obtained from the corresponding author.

3. Numerical procedure

3.1. Material properties

The stress–strain behavior of the model material in this study is characterized by the following power law hardening model:

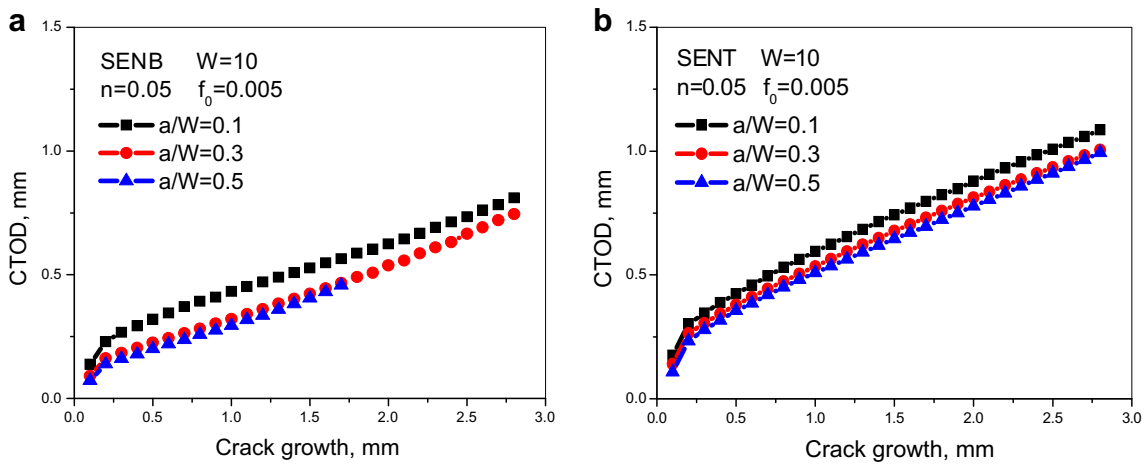

Fig. 3. Resistance curves for $a/W = 0.1$, 0.3 and 0.5, $W = 10$ mm, $L/W = 5$, $n = 0.05$ and $f_0 = 0.005$. (a) SENB; (b) SENT.

Author's personal copy

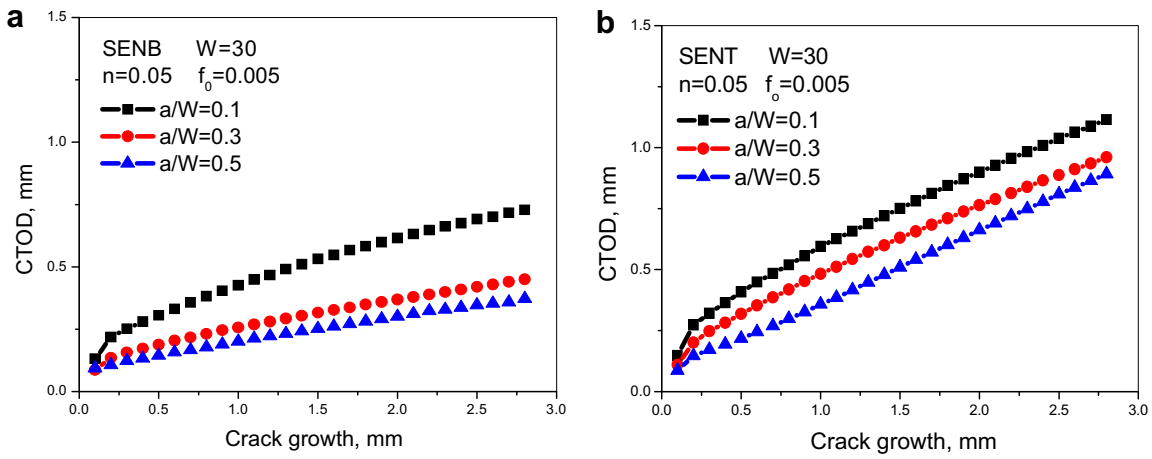

Fig. 4. Resistance curves for $a/W = 0.1$, 0.3 and 0.5, $W = 30$ mm, $L/W = 5$, $n = 0.05$ and $f_0 = 0.005$. (a) SENB; (b) SENT.

$$\sigma_f = \sigma_0\left(1 + \frac{\varepsilon_p}{\varepsilon_0}\right)^n \tag{4}$$

where σ_f is the flow stress which is a function of plastic strain, σ_0 is the yield stress, ε_p is the equivalent plastic strain, ε_0 is the yield strain and n is the strain hardening exponent. The material considered in this study has a yield stress $\sigma_0 = 400$ MPa, Young's modulus $E = 200$ GPa and Poisson ratio $\nu = 0.3$. The effect of initial volume fraction f_0 has also been studied in the analyses. It should be noted that, the material characterized in Eq. (4) is the response in the absence of voids.

3.2. Numerical analyses

The geometrical configurations of specimens are schematically shown in Fig. 2(a) and (b). In all the analyses, the span of the specimen, S, is chosen to be four times the width, W, for SENB ($S/W = 4$) and $L/W = 5$ for SENT specimens.

In order to study the effect of crack tip constraint on ductile fracture behavior, a large variation of crack depths should be covered. Therefore, SENB and SENT specimens with three different crack depths, $a/W = 0.1$, 0.3, and 0.5, are selected for this purpose. Three different specimen widths, $W = 10$, 30 and 50 mm are used to investigate the specimen size effect on resistance curves for both SENB and SENT specimens.

Due to the symmetry, only one half of the specimen was modeled in the finite element analyses and 2D plane strain model with 4-node elements (ABAQUS type CPE4) has been used for the parameter study. A remote homogenous displacement controlled boundary condition (clamped) was applied for the SENT specimen. Large deformation effect is accounted for in all the analyses. The region with uniform element size extends to the width of the specimen and 3.0 mm above the symmetrical interface is used to simulate the ductile crack growth. The element size is 0.1×0.1 mm in this local region except for 0.1×0.05 mm for a single row representing the damage layer along the crack growth path. The finite element mesh and crack tip mesh arrangement in the local region are displayed in Fig. 2(c) and (d). The CTOD-value is extracted from a fixed node in front of the initial crack tip, which can be seen in Fig. 2(e). The element is assumed to fail (e.g. see the deformed elements along the damage layer in front of the crack tip in Fig. 2(e)) when the void volume fraction reaches a certain value f_F, according to the relation $f_F = 0.20 + 2f_0$ used in the complete Gurson model in the present study. Estimating crack growth, Δa, was then executed by multiplying the original element length (0.1 mm) with the number of damaged elements.

4. Results and discussion

In all the analyses, the crack tip opening displacement (CTOD) has been selected as the fracture parameter to describe the crack growth resistance in this study.

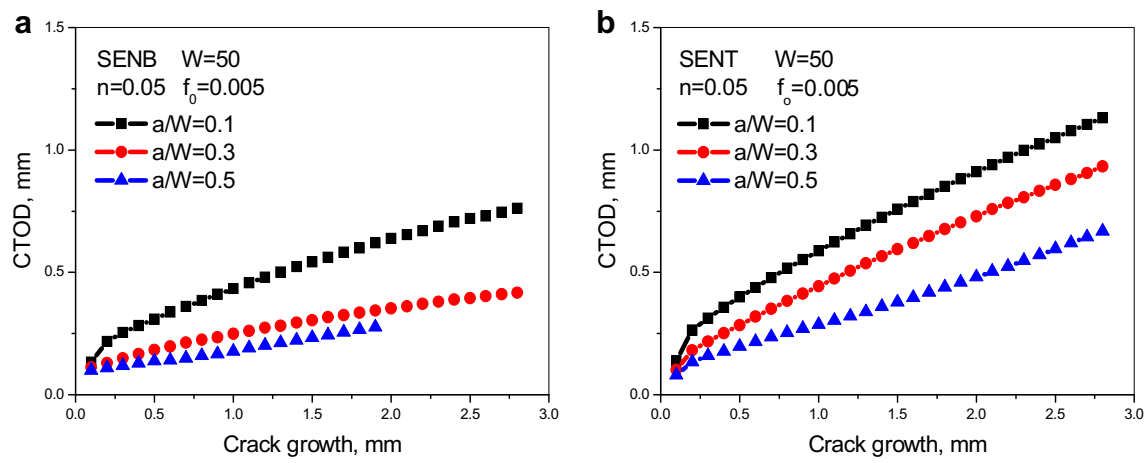

Fig. 5. Resistance curves for $a/W = 0.1$, 0.3 and 0.5, $W = 50$ mm, $L/W = 5$, $n = 0.05$ and $f_0 = 0.005$. (a) SENB; (b) SENT.

Author's personal copy

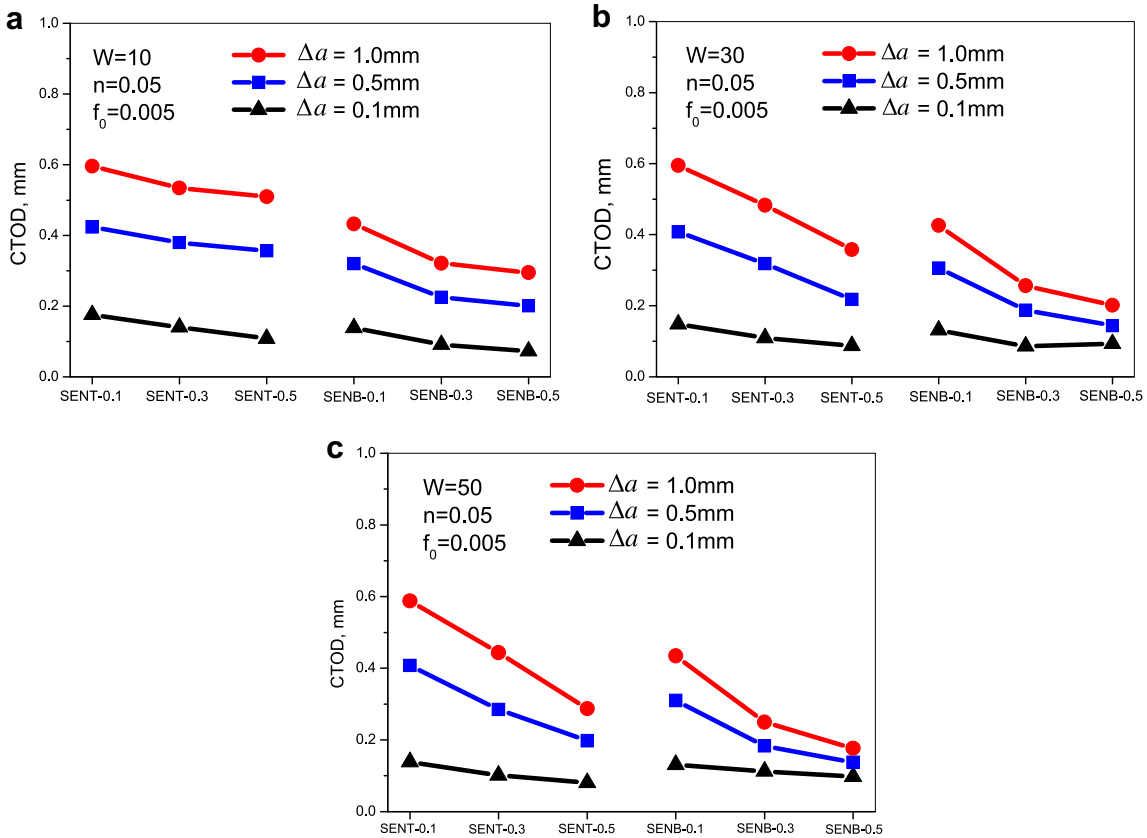

Fig. 6. CTOD versus specimens for $\Delta a = 0.1$, 0.5 and 1.0 mm, $n = 0.05$ and $f_0 = 0.005$. (a) $W = 10$ mm; (b) $W = 30$ mm; (c) $W = 50$ mm.

4.1. Effects of crack depth and loading mode on crack growth resistance curves

The calculated CTOD-resistance curves for both SENB and SENT specimens are presented in Figs. 3–5. In these cases, the strain hardening exponent for the model material considered is $n = 0.05$, and initial void volume fraction is $f_0 = 0.005$.

It can be observed from Figs. 3–5 that, for both SENB and SENT specimens, the CTOD-R curves are comparatively similar at the very beginning for all the models with $W = 10$, 30 and 50 mm. This is consistent with the observations obtained in the previous works [16,34–36], in which a weak dependence of the fracture resistance on crack depth at the onset of crack growth has been found. With further crack growth, a higher resistance curve was obtained for the shallow cracked specimens loaded in both bending and tension. Furthermore, the difference for the resistance curves among the different crack depths becomes gradually larger with the specimen widths increasing from 10 to 50 mm. Similar geometry dependence of the resistance curves has been found for specimens with $W = 50$ mm in [37].

For the same amounts of crack growth, $\Delta a = 0.1$, 0.5 and 1.0 mm, the corresponding CTODs for both SENB and SENT specimens with different crack depths are plotted in Fig. 6. For the initiation toughness ($\Delta a = 0.1$ mm), the effects of crack depth and loading mode are relatively small. With further crack growth, $\Delta a = 0.5$ and 1.0 mm for example, the influence of specimen geometry becomes significant, especially for the larger specimens, as can be seen from Fig. 6(b) and (c). Further results for the specimen size effect will be discussed in the following subsection.

Fig. 7 presents the CTOD values for different specimen sizes with different crack depths at the same crack growth, $\Delta a = 0.5$ mm. It can be found that, for $W = 10$ mm, CTOD-value shows much less dependence on the crack depth for SENT specimens than it does for SENB. This result agrees with the experimental observations by Nyhus et al. [22], which indicates that the fracture toughness of SENT specimens is not sensitive to the initial crack depth. Therefore, it can be concluded that for the small specimens, for example $W = 10$ mm considered in this study, the crack depth has a minor effect on the fracture resistance for SENT specimens. While for the larger specimens, $W = 30$ and 50 mm, the crack depth displays considerable influence on the fracture toughness for both SENB and SENT specimens. Similar experimental results for larger specimens can also be found from [18,38], in which clear differences among

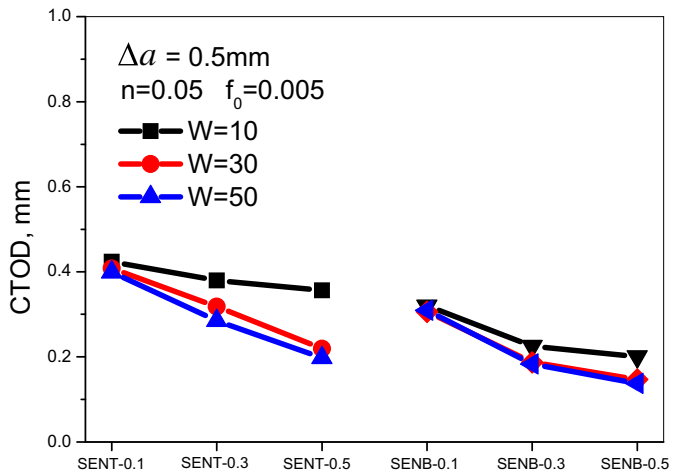

Fig. 7. CTOD versus specimens at $\Delta a = 0.5$ mm. $a/W = 0.1$, 0.3 and 0.5. $n = 0.05$ and $f_0 = 0.005$. $W = 10$, 30 and 50 mm for both SENB and SENT.

Author's personal copy

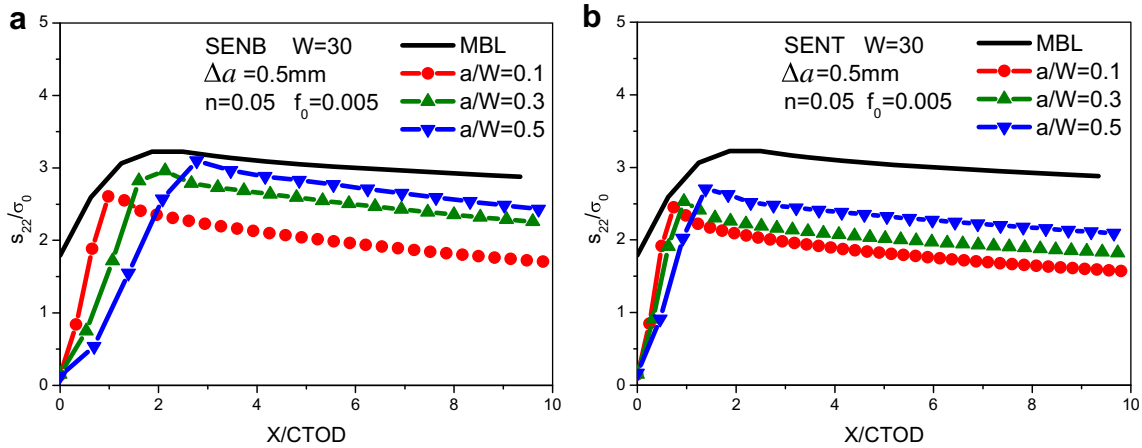

Fig. 8. Opening stress distributions ahead of the crack tip. $n = 0.05$ and $f_0 = 0.005$, $\Delta a = 0.5$ mm. $W = 30$ mm, $a/W = 0.1$, 0.3 and 0.5. (a) SENB; (b) SENT.

the resistance curves has been observed for SENB specimens with $a/W = 0.13$–0.55, $W = 50$ mm.

For better understanding this phenomenon, the Q-parameter [12,13] has been selected to quantify the crack tip constraint for each case. The Q-parameter was originally defined as

$$Q = \frac{\sigma_{\theta\theta} - \left(\sigma_{\theta\theta}^{\mathrm{Ref}}\right)_{T=0}}{\sigma_0}, \quad \text{at} \quad x/(J/\sigma_0) = 2, \ \theta = 0 \tag{5}$$

where $\sigma_{\theta\theta}$ is the opening stress component of interest, $\sigma_{\theta\theta}^{\mathrm{Ref}}$ is the reference stress component characterized by MBL model solution with $T = 0$, x is the distance from the crack tip along the crack plane ($\theta = 0$).

Because of the use of CTOD as the crack driving force in this study, the following definition of Q has been used:

$$Q = \frac{\sigma_{\theta\theta} - \left(\sigma_{\theta\theta}^{\mathrm{Ref}}\right)_{T=0}}{\sigma_0}, \quad \text{at} \quad x/\mathrm{CTOD} = 4, \quad \theta = 0 \tag{6}$$

Only the distribution of the crack tip opening stress ($\sigma_{\theta\theta}$ at $\theta = 0$) has been studied in this paper. One example of the opening stress distribution ahead of the crack tip at $\Delta a = 0.5$ mm for $W = 30$ mm with different crack depths is shown in Fig. 8, together with the reference field obtained from MBL model solution. The distance from the crack tip up to 10 times of the CTOD has been plotted. Fig. 9 displays the calculated CTOD-Q relation for all the specimens loaded in both bending and tension.

It can be found from Fig. 8, the opening stress distribution curves in front of the crack tip are nearly parallel to the reference stress field for both SENB and SENT specimens with various crack depths. Similar results are also observed for other specimen sizes, except a gradual deviation of opening stress distribution from the reference field resulting from the global bending with increasing crack depth for the smallest bending specimens, while the results are not included here for the sake of simplicity.

The corresponding Q values for the smallest SENT specimens, $W = 10$ mm with $a/W = 0.1$, 0.3 and 0.5 in Fig. 9(b), are highly negative and do not change significantly for different crack depths at the same crack growth. This indicates the crack tip constraint is quite low and similar for small SENT specimens with different crack depths for the material considered herein. These specimens therefore exhibit an "independent" relationship between the fracture resistance and crack depth as found in Fig. 3(b). For larger specimens, $W = 30$ and 50 mm, loaded in both bending and tension, CTODs decrease considerably with the increase of crack tip constraint (Q-parameter).

4.2. Near tip stress distribution for growing cracks

For further understanding the effect of crack depth on resistance curves with crack growth, Figs. 10–12 present the opening stress distribution ahead of the crack tip for all the specimens with different sizes and crack depths at $\Delta a = 0.1$, 1.0 and 2.0 mm respectively.

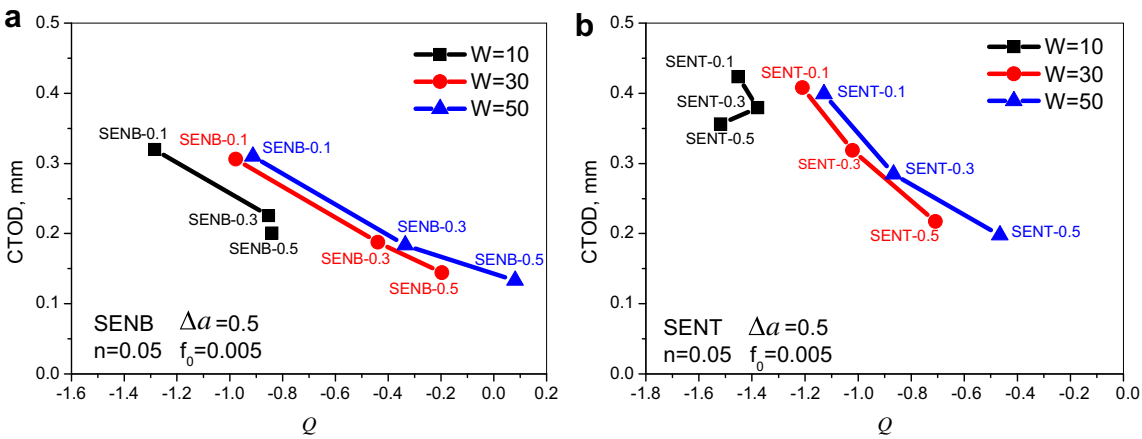

Fig. 9. CTOD-Q relation. $n = 0.05$, $f_0 = 0.005$, $\Delta a = 0.5$ mm. $a/W = 0.1$, 0.3 and 0.5. $W = 10$, 30 and 50 mm. (a) SENB; (b) SENT.

Author's personal copy

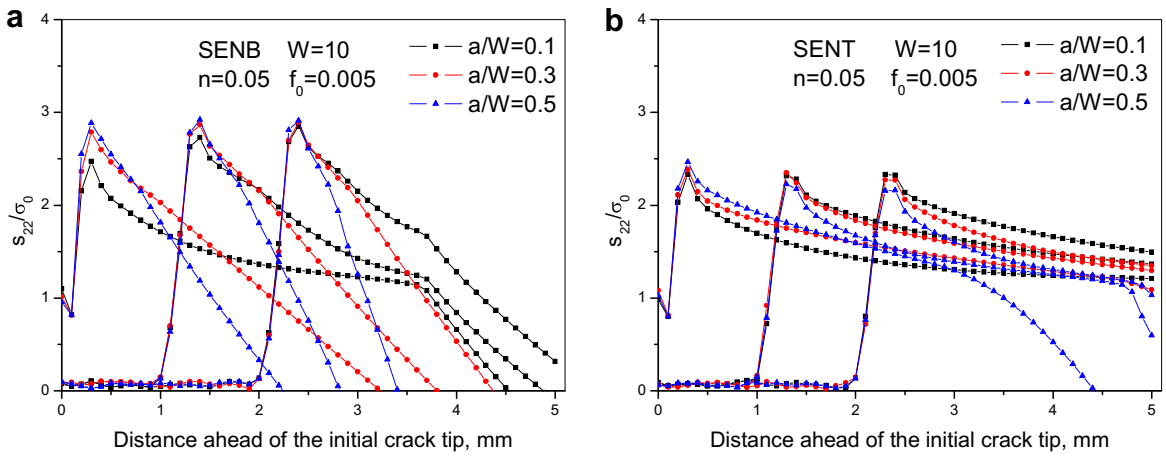

Fig. 10. Effects of crack growth and crack depth on opening stress distribution ahead of the crack tip. $n = 0.05$, $f_0 = 0.005$, $W = 10$. (a) SENB; (b) SENT.

For the SENT specimens with $W = 10$ mm, it can be seen in Fig. 10(b) that, the peak stresses in front of the crack tip show a relatively small dependence on the crack depths with further crack growth. For the cases with $W = 30$ and 50 mm in Figs. 11 and 12, a much more evident effect of crack depths on the opening stress distribution can be seen for both SENB and SENT specimens. Moreover, the difference in peak stress among different crack depths increases with the increase of specimen sizes at the same crack growth, which again explain the gradually larger effect of crack depths on the resistance curves with increasing specimen sizes. For most of the cases, specimens with the smallest crack depth, $a/W = 0.1$, show the lowest peak stress at the same crack growth, therefore yields the highest resistance curve, as have been shown above in Figs. 3–5. The peak stress slightly increases with further crack growth for a given specimen size for most of the cases. Similar results can also be found in a previous work [39]. While for SENT specimens with $a/W = 0.5$, a somewhat reduced peak stress with crack growth can be found.

4.3. Effect of specimen size on crack growth resistance curves

In this subsection, further discussion will be focused on the specimen size effect on the crack growth resistance. Fig. 13 shows the calculated CTOD-R curves for shallow ($a/W = 0.1$) and deep ($a/W = 0.5$) cracked specimens loaded in bending and tension.

For the cases with $a/W = 0.1$, it can be clearly seen from Fig. 13(a) and (b) that there is less dependence of resistance curves on specimen sizes for both bending and tension specimens. Therefore, the fracture toughness can be directly transferred from small specimen to the larger ones for crack growth no more than 2.5 mm for SENB and 2.8 mm for SENT specimens for material considered here. This result shows a small deviation from a previous work [40], in which there is a weak dependence of resistance curves on specimen sizes with regard to ductile crack growth less than 1–1.5 mm and then the size effect starts to become relatively evident with further crack growth. Different crack driving force used for calculating the resistance curves could be the reason for this difference. In the previous work [40], J-integral was selected as the crack driving force parameter, while in this study the CTOD was used for all the analyses. It is beyond the scope of this paper to discuss which parameter is the more appropriate one.

For $a/W = 0.5$, however, a more pronounced specimen size effect on crack growth resistance has been observed for both SENB and SENT specimens, Fig. 13(c) and (d). The crack growth resistance increases with the decrease of specimen size. This increase in toughness is associated with a loss of constraint as the specimen size is reduced, which can be seen from Fig. 9. Similar findings for the effect of specimen size on the J–Δa curves have also been reported for specimens loaded in bending in [40].

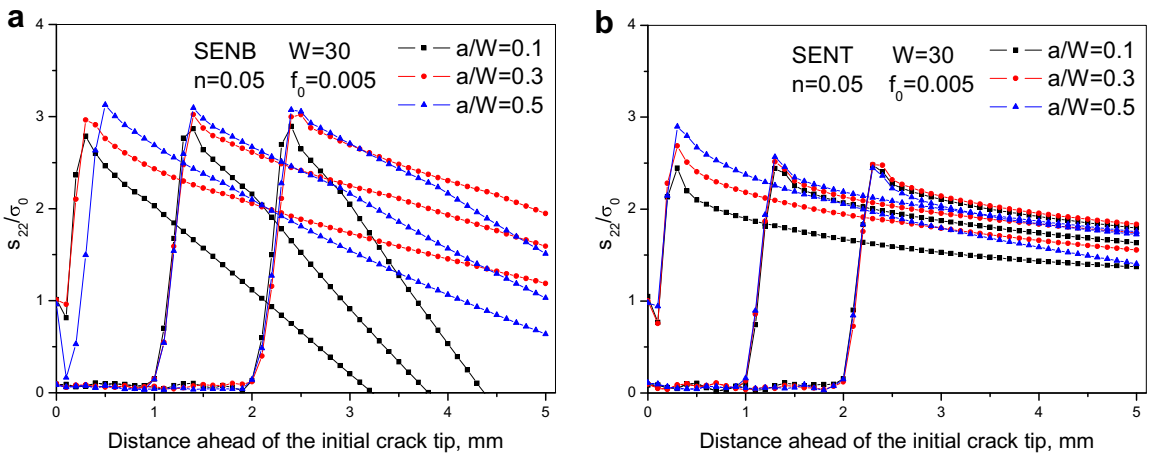

Fig. 11. Effects of crack growth and crack depth on opening stress distribution ahead of the crack tip. $n = 0.05$, $f_0 = 0.005$, $W = 30$. (a) SENB; (b) SENT.

Author's personal copy

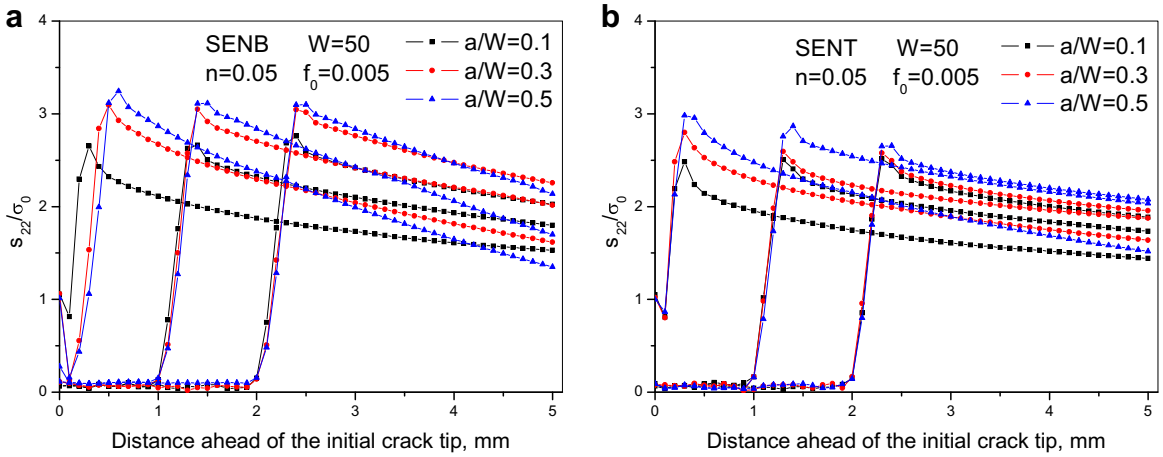

Fig. 12. Effects of crack growth and crack depth on opening stress distribution ahead of the crack tip. $n = 0.05$, $f_0 = 0.005$, $W = 50$. (a) SENB; (b) SENT.

The different effects of the specimen size on resistance curves for shallow ($a/W = 0.1$) and deep ($a/W = 0.5$) cracked cases can be well explained by the opening stress distribution ahead of crack tip as displayed in Fig. 14.

For $a/W = 0.1$ for both SENB and SENT specimens, specimen size has very limited effect on the peak stress with crack growth, Fig. 14(a) and (b), which therefore explains the small or virtually no influence of specimen size on the resistance curves as have been found in Fig. 13(a) and (b).

For $a/W = 0.5$, Fig. 14(c) and (d), a significant effect of specimen size on the peak stress ahead of the crack tip can be seen, thereby illustrating the pronounced specimen size effect on crack growth resistance as have been observed in Fig. 13(c) and (d). Moreover, the stress level ahead of the crack tip increases with increasing specimen size, thus a decrease in crack growth resistance should be expected with the increase of specimen size.

4.4. Effect of initial void volume fraction

The effects of crack depth and specimen size may depend on the material toughness. For this consideration, model material with lower initial void volume fraction, 10% of the previous value used,

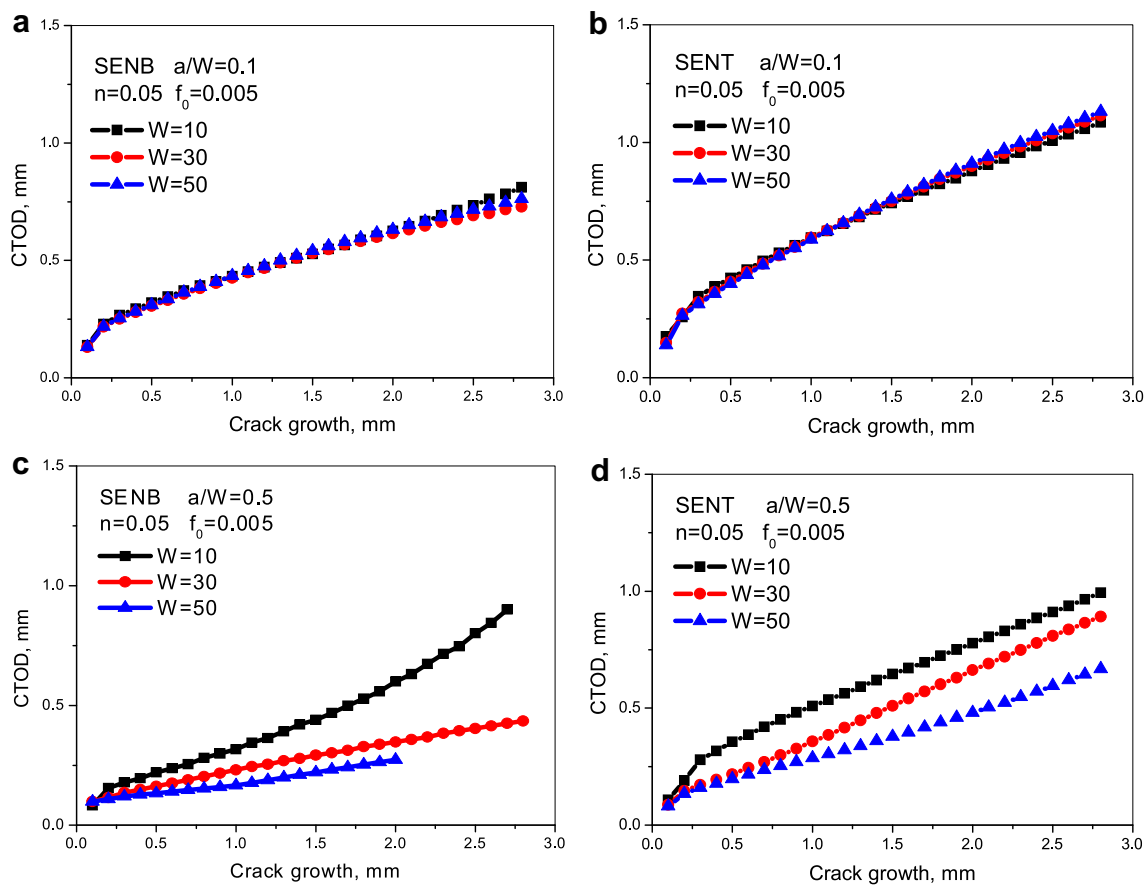

Fig. 13. The effect of specimen size on the CTOD–Δa curves. $n = 0.05$ and $f_0 = 0.005$. (a) $a/W = 0.1$, SENB; (b) $a/W = 0.1$, SENT; (c) $a/W = 0.5$, SENB; (d) $a/W = 0.5$, SENT.

Author's personal copy

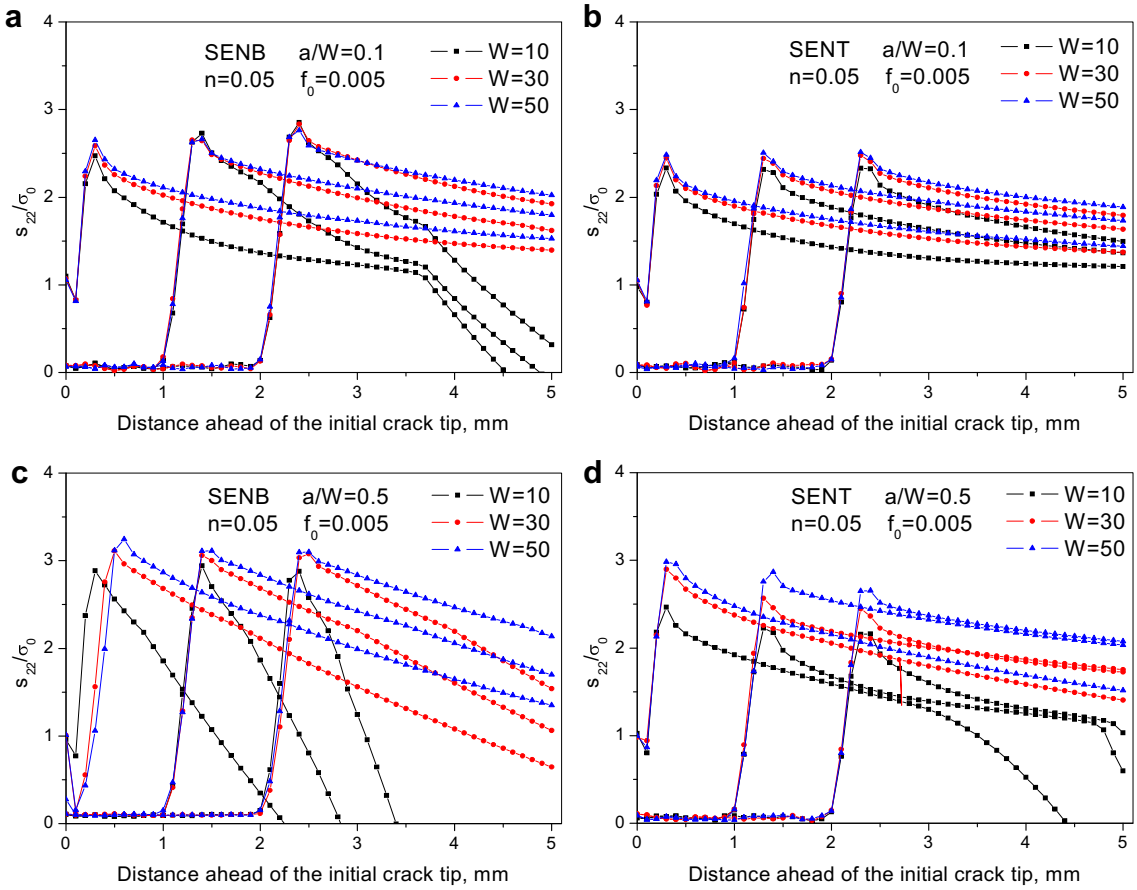

Fig. 14. Effects of crack growth and specimen size on opening stress distribution ahead of the crack tip. (a) $a/W = 0.1$, SENB; (b) $a/W = 0.1$, SENT; (c) $a/W = 0.5$, SENB; (d) $a/W = 0.5$, SENT.

which means higher material toughness, has been analyzed. Fig. 15 presents the results for both SENB and SENT specimens with $W = 50$ mm.

It can be seen that, for model material with lower initial void volume fraction $f_0 = 0.0005$, significantly higher resistance curves are obtained compared with the cases with $f_0 = 0.005$. Moreover, the effect of crack depth on the resistance curves becomes smaller than the cases with $f_0 = 0.005$, especially for SENB specimens with relative deep cracks, $a/W = 0.3$ and $a/W = 0.5$. Similar trends can also be obtained for other specimens with smaller sizes, $W = 10$ and 30 mm. Therefore, the influence of crack depth on resistance curves is strongly related to the material toughness. A weaker dependence of crack growth resistance on crack depth can be expected for material with higher fracture toughness.

In addition, the specimen size effect for the cases with $a/W = 0.5$ and lower initial void volume fraction, $f_0 = 0.0005$, are displayed in Fig. 16. It can be clearly observed that, for the material with $f_0 = 0.0005$ and other parameters are fixed, remarkably higher crack growth resistance than the cases with $f_0 = 0.005$ can be

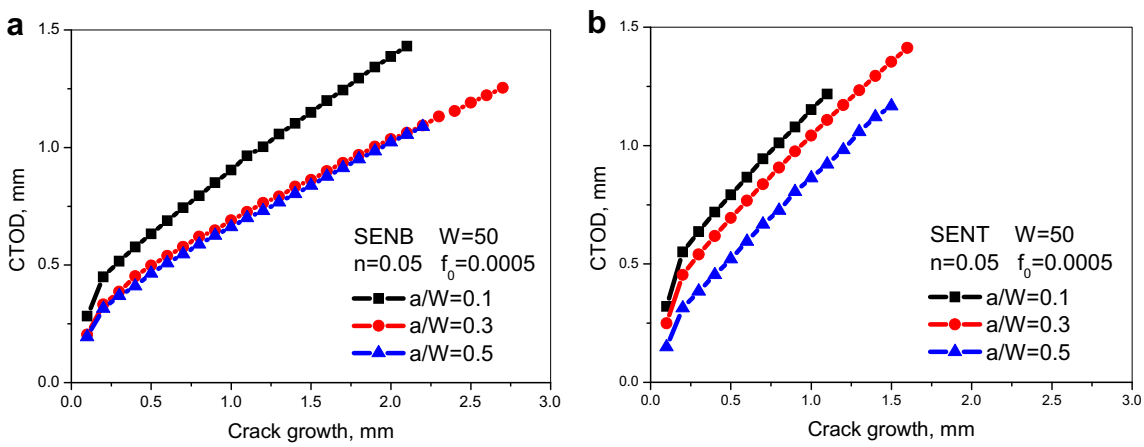

Fig. 15. Resistance curves for $a/W = 0.1$, 0.3 and 0.5, $W = 50$ mm, $n = 0.05$ and $f_0 = 0.0005$. (a) SENB; (b) SENT.

Author's personal copy

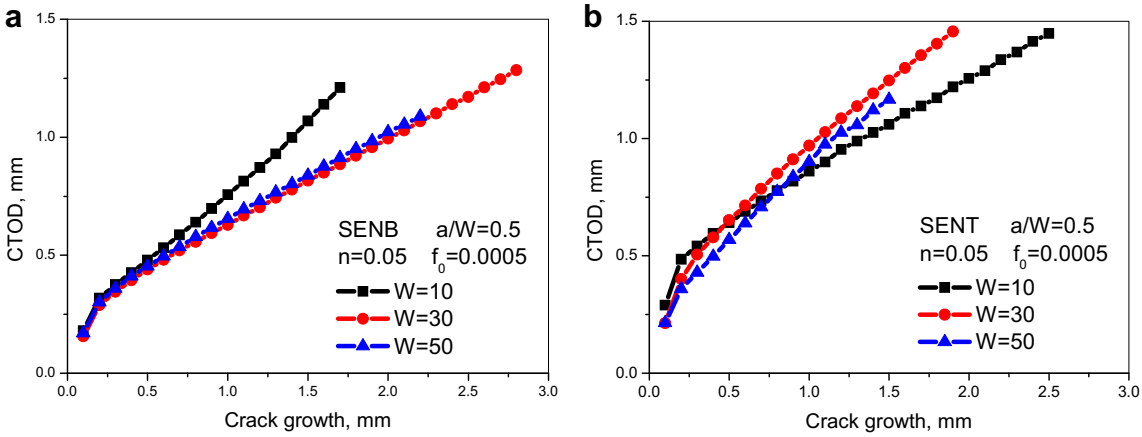

Fig. 16. The effect of specimen size on the CTOD–Δa curves. $n = 0.05, f_0 = 0.0005$. $W = 10$, 30 and 50 mm. (a) SENB; (b) SENT.

found. It also shows that the effect of specimen sizes on resistance curves becomes smaller for both SENB and SENT specimens.

With further crack extension, the smallest specimen, $W = 10$ mm, displays a markedly higher crack growth resistance. The other two larger specimens, $W = 30$ and 50 mm, however, show less size effect on the resistance curves for SENB as can be seen from Fig. 16(a). As for tension specimens in Fig. 16(b), it can be seen that the influence of specimen size on crack growth resistance curves becomes smaller compared with that of models with $f_0 = 0.005$ in Fig. 13(d).

The effect of specimen size for both shallow ($a/W = 0.15$) and deep ($a/W = 0.5$) cracks and material hardening on ductile crack growth resistance have been studied in [39,40]. The results show that the effect of specimen size for both shallow and deep cracks depends strongly on the material hardening. For low hardening (large plasticity), the effects of both specimen geometry and size are more significant. When the material displays a high hardening, both the geometry and size effects are strongly reduced. Therefore, it can be concluded that, both initial void volume fraction and hardening level have strong influence on the effects of specimen geometry and size on ductile crack growth resistance.

5. Concluding remarks

The complete Gurson model has been used to predict ductile crack growth resistance curves. 2D plane strain FE analyses have been carried out to study the effects of crack depth and specimen size on ductile crack growth behavior for both SENB and SENT specimens which were used to experimentally characterize the thin-walled pipeline steels.

It has been observed that, the smallest SENT specimens exhibit the lowest crack tip constraint level (large negative Q) and display a small difference in Q-values for different crack depths, indicating a weak dependence of the CTOD resistance curves on crack depth.

As for larger specimens, $W = 30$ and 50 mm, a dependence of Q-parameter on crack depth has been obtained, which explains the significant influence of crack depth on the resistance curves for both SENB and SENT specimens.

With regard to the specimen size effect on the ductile crack growth resistance, it has been found that CTOD resistance curves display less dependence on the specimen size for shallow cracked specimens, $a/W = 0.1$, loaded in both bending and tension. While a more pronounced size effect can be seen with further crack growth for the deep cracked specimens, $a/W = 0.5$, for both SENB and SENT.

However, it should be noted that, the effects of crack depth and specimen size on resistance curves are strongly related to the material toughness level, as denoted by the initial void volume fraction f_0, and the strain hardening as well. These effects will be significantly reduced for the material with a higher toughness level and/or higher hardening.

Acknowledgments

The first author sincerely thanks to the financial support from the China Scholarship Council.

References

[1] Wallin K. The size effect in K_{IC} results. Eng Fract Mech 1985;22:149–63.
[2] Sorem WA, Dodds RH, Rolfe ST. Effects of crack depth on elastic-plastic fracture toughness. Int J Fract 1991;47:105–26.
[3] Aurich D, Sommer E. The effect of constraint on elastic-plastic fracture. Steel Res 1988;59:358–67.
[4] Yuan H, Brocks W. Quantification of constraint effects in elastic-plastic crack front field. J Mech Phys Solids 1998;46:219–41.
[5] Dodds RH, Shih CF, Anderson TL. Continuum and micromechanics treatment of constraint in fracture. Int J Fract 1993;64:101–33.
[6] Nevalainen M, Dodds RH. Numerical investigation of 3-D constraint effects on brittle fracture in SE (B) and C(T) specimens. Int J Fract 1995;74:131–61.
[7] Dodds RH, Ruggieri C, Koppenhoefer KC. ASTM STP 1321. In: Underwood JH, Macdonald BD, Mitchell MR, editors. 3-D constraint effects on models for transferability of cleavage fracture toughness. Fatigue and fracture mechanics, vol. 28. Philadelphia: American Society for Testing and Materials; 1997. p. 179–97.
[8] Zhang ZL, Hauge M, Thaulow C. Two-parameter characterization of near-tip fields of a bi-material elastic-plastic interface crack. Int J Fract 1996;79:65–83.
[9] Zhang ZL, Thaulow C, Hauge M. Effect of crack size and weld metal mismatch on the cleavage toughness of wide plates. Eng Fract Mech 1997;57(6):653–64.
[10] Liu J, Zhang ZL, Nyhus B. Residual stress induced crack tip constraint. Eng Fract Mech 2008;75(14):4151–66.
[11] Betegon C, Hancock JW. Two-parameter characterization of elastic–plastic crack-tip fields. J Appl Mech 1991;58:104–10.
[12] O'Dowd NP, Shih CF. Family of crack-tip fields characterized by a triaxiality parameter-I. Structure of fields. J Mech Phys Solids 1991;39(8):989–1015.
[13] O'Dowd NP, Shih CF. Family of crack-tip fields characterized by a triaxiality parameter-II. Fracture applications. J Mech Phys Solids 1992;40(5):939–63.
[14] Shih CF, O'Dowd NP, Kirk MT. A framework for quantifying crack tip constraint. ASTM STP 1171. In: Hackett EM, Schwalbe KH, Dodds RH, editors. Constraint effects in fracture. Philadelphia: American Society for Testing and Materials; 1993. p. 2–20.
[15] Brocks W, Schmitt W. Quantitative assessment of the role of crack tip constraint on ductile tearing. ASTM STP 1171. In: Hackett EM, Schwalbe KH, Dodds RH, editors. Constraint effects in fracture. Philadelphia: American Society for Testing and Materials; 1993. p. 64–78.
[16] Hancock JW, Reuter WG, Parks DM. Constraint and toughness parameterized by T. ASTM STP 1171. In: Hackett EM, Schwalbe KH, Dodds RH, editors. Constraint effects in fracture. Philadelphia: American Society for Testing and Materials; 1993. p. 21–40.
[17] O'Dowd NP, Shih CF. ASTM STP 1207. In: Landes JD, McCabe DE, Boulet JAM, editors. Two-parameter fracture mechanics: theory and applications. Fracture mechanics, vol. 24. Philadelphia: American Society for Testing and Materials; 1994. p. 21–47.

Author's personal copy

[18] Joyce JA, Link RE. ASTM STP 1256. In: Reuter WG, Underwood JH, Newman JC, editors. Effects of constraint on upper shelf fracture toughness. Fracture mechanics, vol. 26. Philadelphia: American Society for Testing and Materials; 1995. p. 142–77.
[19] Xu J, Zhang ZL, Østby E, Nyhus B, Sun DB. Constraint effect on the ductile crack growth resistance of circumferentially cracked pipes. Eng Fract Mech, in press, doi:10.1016/j.engfracmech.2009.11.005.
[20] Nyhus B, Østby E, Thaulow C, Zhang ZL, Olden V. SENT testing and the effect of geometry constraint in high strength steel. In: International symposium high strength steel, Verdal, Norway; 2002.
[21] Nyhus B, Polance ML, Ørjasæter O. SENT specimens an alternative to SENB specimens for fracture mechanics testing of pipelines. In: Proceedings of OMAE2003, the 22nd international conference on offshore mechanics and arctic engineering, Cancun, Mexico; 2003.
[22] Nyhus B, Østby E, Knagenhjelm HO, Black S, Røstadsand PA. Experimental studies on the effect of crack length and asymmetric geometries on the ductile tearing resistance. In: Proceedings of OMAE2005, the 24th international conference on offshore mechanics and arctic engineering, Halkidiki, Greece; 2005.
[23] Recommended practice DNV-RP-F108. Fracture control for pipeline installation methods introducing cyclic plastic strain; 2006.
[24] Zhang ZL, Thaulow C, Ødegård J. A complete Gurson model approach for ductile fracture. Eng Fract Mech 2000;67:155–68.
[25] Gurson AL. Plastic flow and fracture behavior of ductile materials incorporating void nucleation, growth and coalescence. PhD dissertation, Brown University; 1975.
[26] Tvergaard V. Influence of voids on shear band instabilities under plane strain conditions. Int J Fract 1981;17:389–407.
[27] Tvergaard V. On localization in ductile materials containing spherical voids. Int J Fract 1982;18:237–52.
[28] Tvergaard V, Needleman A. Analysis of the cup-core fracture in a round tensile bar. Acta Metall 1984;32:157–69.
[29] Thomason PF. Ductile fracture of metals. Oxford: Pergamon Press; 1990.
[30] ABAQUS user manual. ABAQUS; 2007. version 6.7-1.
[31] Zhang ZL, Niemi E. A class of generalized mid-point algorithms for Gurson–Tvergaard continuum damage material model. Int J Numer Methods Eng 1995;38:2033–53.
[32] Zhang ZL. On the accuracies of numerical integration algorithms for Gurson pressure-dependent elastoplastic constitutive models. Comput Meth Appl Mech Eng 1995;121:15–28.
[33] Zhang ZL. Explicit consistent tangent moduli with a return mapping algorithm for pressure-dependent elastoplasticity models. Comput Meth Appl Mech Eng 1995;121:29–44.
[34] Tvergaard V, Hutchinson JW. Effect of T-stress on mode I crack growth resistance in a ductile solid. Int J Solids Struct 1994;31:823–33.
[35] Xia L, Shih CF. Ductile crack growth-I: a numerical study using computational cells with microstructurally-based length scales. J Mech Phys Solids 1995;43(2):223–59.
[36] Joyce JA, Link RE. Effects of tensile loading on upper shelf fracture toughness. NU-REG/CR-6051. U.S. Nuclear Regulatory Commission; 1994.
[37] Xia L, Shih CF. Ductile crack growth-II: void nucleation and geometry effects on macroscopic fracture. J Mech Phys Solids 1995;43(12):1953–81.
[38] Joyce JA, Link RE. Application of two parameter elastic-plastic fracture mechanics to analysis of structures. Eng Fract Mech 1997;57(4):431–46.
[39] Østby E, Thaulow C, Zhang ZL. Numerical simulation of specimen size and mismatch effects in ductile crack growth-part II: near-tip stress fields. Eng Fract Mech 2007;74:1793–809.
[40] Østby E, Thaulow C, Zhang ZL. Numerical simulation of specimen size and mismatch effects in ductile crack growth-part I: tearing resistance and crack growth paths. Eng Fract Mech 2007;74:1770–92.